0026-895X/05/6703-714–720$20.00
MOLECULAR PHARMACOLOGY

Mol Pharmacol 67:714–720, 2005

Vol. 67, No. 3
8888/11895623
Printed in U.S.A.

The Aryl Hydrocarbon Receptor Is Required for Developmental Closure of the Ductus Venosus in the Neonatal Mouse[S]

Garet P. Lahvis, Robert W. Pyzalski, Edward Glover, Henry C. Pitot, Matthew K. McElwee, and Christopher A. Bradfield

Departments of Surgery (G.P.L., M.K.M.) and Radiology (R.W.P.) and McArdle Laboratory for Cancer Research (E.G., H.C.P., C.A.B.), University of Wisconsin Medical School, Madison, Wisconsin

Received November 2, 2004; accepted December 7, 2004

ABSTRACT

A developmental role for the *Ahr* locus has been indicated by the observation that mice harboring a null allele display a portocaval vascular shunt throughout life. To define the ontogeny and determine the identity of this shunt, we developed a visualization approach in which three-dimensional (3D) images of the developing liver vasculature are generated from serial sections. Applying this 3D visualization approach at multiple developmental times allowed us to demonstrate that the portocaval shunt observed in *Ahr*-null mice is the remnant of an embryonic structure and is not acquired after birth. We observed that the shunt is found in late-stage wild-type embryos but closes during the first 48 h of postnatal life. In contrast, the same structure fails to close in *Ahr*-null mice and remains open throughout adulthood. The ontogeny of this shunt, along with its 3D position, allowed us to conclude that this shunt is a patent developmental structure known as the ductus venosus (DV). Upon searching for a physiological cause of the patent DV, we observed that during the first 48 h, most major hepatic veins, such as the portal and umbilical veins, normally decrease in diameter but do not change in *Ahr*-null mice. This observation suggests that failure of the DV to close may be the consequence of increased blood pressure or a failure in vasoconstriction in the developing liver.

The *Ahr* locus encodes the aryl hydrocarbon receptor (AHR), a basic-helix-loop helix *Per-Arnt-Sim* protein that is best known for its role in mediating biological responses to halogenated dioxins and related toxic and carcinogenic environmental chemicals (Mimura and Fujii-Kuriyama, 2003). We reported recently that this protein also plays an important role in vascular biology (Lahvis et al., 2000). Although *Ahr*-null mice are viable, the liver size in these animals is approximately 30% smaller than that of wild-type control mice. This hepatic phenotype is fully penetrant and is found in both adult male and female mice. Morphometric analysis indicates that the smaller liver is partially the result of decreased hepatocyte size (Lahvis et al., 2000). Our investigations into the cause of the smaller liver led to the discovery that adult *Ahr*-null animals suffer from portocaval shunting of blood within the liver parenchyma. Using adult mice, studies with micro-spheres indicate that more than half of the portal blood that flows to the liver bypasses the liver sinusoids in *Ahr*-null mice (Lahvis et al., 2000). Latex-corrosion casts and time-lapse angiography in adult mice demonstrate that this bypass results from a single direct shunt between the portal vein (PV) and the inferior vena cava (IVC) (Lahvis et al., 2000).

We have been interested in the identity of the portocaval shunt observed in adult *Ahr*-null mice, as well as its physiological cause. The purpose of this study was to formally examine whether the shunt was congenital or acquired. As a result of our previous work, we postulated that this shunt might be a congenital phenomenon, the result of a patent fetal vascular structure known as the ductus venosus (DV) (Lahvis et al., 2000). The DV shunts umbilical blood through the liver to the IVC. Given that all of our prior analysis has been performed using adult animals, it is equally possible that this shunt was acquired as the result of some aberrant liver physiology/pathology (for example, through the formation of collateral blood vessels related to portal hypertension) (Datta et al., 1975; Sugiura et al., 1992).

To distinguish between possible congenital or acquired causes of this portocaval shunt, we set out to understand the

Financial support for this study was provided by National Institutes of Health grants P30-CA014520, P01-CA022484, F32-ES05887 and in part by a University of Wisconsin Department of Surgery Research Grant.

[S] The online version of this article (available at http://molpharm.aspetjournals.org) contains supplemental material.

Article, publication date, and citation information can be found at http://molpharm.aspetjournals.org.
doi:10.1124/mol.104.008888.

ABBREVIATIONS: AHR, aryl hydrocarbon receptor; PV, portal vein; IVC, inferior vena cava; DV, ductus venosus; 3D, three-dimensional; UV, umbilical vein; DA, ductus arteriosus.

precise three-dimensional (3D) position of this structure and how it changes over developmental time. To accomplish this objective, we evaluated the ontogeny of this shunt in wild-type and *Ahr*-null mice by reconstructing 3D volumes of the liver vasculature at multiple prenatal and postnatal developmental times. Using this approach, we confirmed that the position and ontogeny of the portocaval shunt in *Ahr*-null mice is consistent with its identity as a patent DV and that this structure is not the result of a shunt that is acquired later in life. Moreover, we provide preliminary evidence that the patent DV may be the result of reduced vascular tone in the developing *Ahr*-null liver.

Materials and Methods

Mice. The *Ahr*-null mouse colony (designated $Ahr^{-/-}$) used in these studies were congenic to the C57BL/6J (B6) background. This colony was generated by 20 backcrosses to the B6 strain (N20) with continual selection for the Ahr^{-} allele. The $Ahr^{-/-}$ (null) and $Ahr^{+/+}$ (wild-type) control mice were derived from intercrosses of $Ahr^{+/-}$ heterozygotes. All animals received humane care according to the criteria outlined in the *Guide for the Care and Use of Laboratory Animals* (http://www.nap.edu/readingroom/books/labrats/).

Caesarian Derivation. To establish the exact time of birth, mice were delivered by caesarian derivation at embryonic day 18.5. In brief, the abdomen was incised, the uterus was removed, and fetuses were isolated from the visceral yolk sac and amnion. Pups were palpated with sterile cotton-tipped swabs to facilitate breathing. For fostering, pups were mixed with pups of a foster dam and when possible, with maternal urine. Pups of the foster dam were then removed and the foster dam was returned to the cage with the caesarian-derived animals.

Liver Isolation and Fixation. At specific times after caesarian delivery, liver, lung, kidneys, stomach, and intestines were quickly excised from euthanized newborn mice as a single unit. These organs were then dipped in 10% (v/v) neutral buffered formalin and suspended by the lungs to achieve a mild fixation of the liver lobes that reflected their natural position within the abdomen. Organs were then placed in 10% neutral buffered formalin and maintained at 4°C overnight. After fixation, organs were rinsed and stored in chilled ethanol/H_2O (70:30). Fixed livers were then dissected from the lungs and inferior regions of the small intestines. Care was taken to maintain the umbilical vein, suprahepatic IVC, and portion of the diaphragm proximal to the IVC. Portions of the intestine and kidney were dissected to help in the identification of the infrahepatic PV and IVC, respectively. Stomach contents were removed to minimize effects of stomach acids on hematoxylin and eosin staining. Livers were embedded with the diaphragm, and suprahepatic IVC placed proximal to the bottom of the wax boat. Transverse serial sectioning began at the diaphragm and proceeded through to the kidneys. Serial 5-μm liver sections were obtained and digitally photographed, producing either 1090 $\times$ 1300-pixel images (using a Zeiss Axiocam on a Zeiss Axioplan 2 microscope) or 240 $\times$ 460-pixel images (using an Olympus OLY-750 CCD camera and an IBM-compatible PC with a frame-grabber card through a Navitar zoom 7000 lens).

Three-Dimensional Reconstruction. Three-dimensional reconstruction requires the alignment and stacking of digital photographs of serial sections. Alignment is necessary for reconstruction from histological sections, because they are placed by hand on glass slides in a water bath. As a result, the orientation of each section relative to the glass slide is variable, and photographs of each slide provide a range of orientations. Therefore, image-processing software was used to help align serial sections. This image registration procedure was performed on consecutive pairs of images throughout each stack (e.g., section 1 and 2, then 2 and 3, etc.). The overlying section was first adjusted so that its center approximately overlapped that of the previous section. We then rotated the overlying image to re-establish the continuity of the majority of points from section to section. When all of the sections were aligned with one another, they were then combined into one 3D image file for each sample. The software that was used to align sections and stack them into a 3D image file was written in our lab, using VolPack (Lacroute and Levoy, 1994), and the XIL and XView libraries. The processing was done on a Sun Ultra 1 workstation running the Solaris operating system.

Projection images and movies of the 3D reconstructions were produced using Voxx, a volume rendering program that permits examination and manipulation of a stack of aligned two-dimensional images in near real-time on a PC (Clendenon et al., 2002). Nonlinear intensity transformations and intensity-to-color mappings were used to improve the visibility of the vessels (Clendenon et al., 2002). Scale factors for the 3D images were computed using images of a stage micrometer slide and the thickness of the tissue sections. Examples of 3D images generated with Voxx are provided in Figs. 2 and 4. To improve our ability to see of the vessels within the liver, the axis perpendicular to the plane of section was increased 3-fold relative to X and Y dimensions.

Fluorescence Imaging. To characterize the vascular structures of the neonatal brain, we stained the luminal surface of the vessels with a fluorescent-labeled lectin derived from the tomato *Lycopersicon esculentum* (McDonald et al., 1999) (Vector Laboratories, Burlingame, CA). The intravascular space of a neonatal mouse was accessed by insertion of a pulled glass pipette (outer diameter, ~50 um) into the aortic arch. We used a micromanipulator to direct the pipette tip into the vessel and tie the vessel to the tip with a 10-0 suture. The descending aorta was occluded and the right atrium was incised. The neonatal brain was stained and fixed during the perfusion. Thick sections (75 μm) are obtained with a vibrating microtome, and images were collected by fluorescence microscopy.

Vessel Diameters. The diameters of the IVC, PV, and umbilical vein (UV) were determined at their sites of entry to the liver. Measurements were typically taken from at least three individual samples at each time-point. Three measurements of vessel diameter were collected from section photographs at 15-μm intervals from the site where the vessel was encapsulated by the liver. Measurements of DV diameter were made at the intrahepatic site, where the DV was narrowest. Measurements were calibrated with a stage micrometer, and analysis of variance was used for statistical comparison of vessel diameters (Sokal and Rohlf, 1995).

Results

Identification of Major Hepatic Veins. Identification of the DV in newborn mice was accomplished by its unique vascular connections. The DV is the only fetal vessel that shunts blood to the IVC and to the PV, thereby providing retrograde perfusion of the liver (see Fig. 1A). To locate the DV, we first identified the fetal UV, PV, and the IVC as reference vascular structures within the liver. Each of these vessels was identified by virtue of their distinct anatomical characteristics and position of entry into the developing liver. The PV is a relatively small vessel that drains the esophagus, stomach, intestines, spleen, pancreas, and gall bladder. The PV enters the liver via a central site, adjacent to the hepatic artery, between the right and left lobes. A transverse section through its liver entry point is shown (Fig. 1B). The UV enters the median lobe of the liver, adjacent to the gall bladder and associated bile duct, and typically narrows as it enters the liver (Fig. 1C). The infrahepatic IVC is associated with renal veins inferior to the liver and enters to the liver via the distal region of the right lobe (Fig. 1D). The suprahepatic IVC leaves the liver and traverses the diaphragm (Fig. 1E).

Vascular Anatomy of Neonatal Liver Can Be Described by 3D Reconstruction. To visualize the hepatic blood vessels by 3D reconstruction, we began by highlighting all of the blood vessels of greater than ~25 μm in diameter in each section. In every section through the liver, standard thresholding tools were employed to delineate the vascular lumen from surrounding parenchyma (e.g., "clear" versus "stained"). Vessel lumens were highlighted in black, and photographs were then converted from RGB to gray-scale format. In the final reconstructions used to generate figures, the gray scale was inverted so that vessels are visible as white structures in gray parenchyma on a black background.

Figure 2 provides an example of the flexibility, quality, and resolution of the 3D images generated by this approach. These two-dimensional images represent "screen shots" from different turns of the 3D images generated by reconstruction of the major hepatic blood vessels of a wild-type mouse at 24 h of age. By modifying threshold values from the reconstruction, we are able to see either the surface of the tissue, in this case the abdominal cavity and its associated organs (Fig. 2A), or a similarly positioned internal vascular pattern that highlights only the hepatic vasculature (Fig. 2B). Surface imaging shows the liver (L) from different angles, allowing us to see the associated diaphragm (D), spleen, kidneys, and intestine (Fig. 2A). Surface imaging also allows us to see the renal veins at the inferior end of the reconstruction and the suprahepatic IVC as it leaves the diaphragm. When we change threshold settings for the volume, the surface image becomes a faint "ghost", and we can visualize the large hepatic vessels that have been highlighted (Fig. 2B). We can clearly identify the IVC, which runs from the kidneys through the liver, and the UV from several orientations. However, the PV and DV remain obscured by many vessel branches that proceed through the liver lobes. Examples of Voxx-rendered videos highlighting abdominal organ morphology (Supplemental Fig. 1) and hepatic vasculature (Supplemental Fig. 2) are available for viewing.

To identify the DV, we relied upon its distinct anatomy as the only vessel that connects the fetal PV, UV, and IVC. All other hepatic vascular structures emanate from these larger vessels and then continue to branch, forming much finer structures that terminate in the distal regions of the liver. To facilitate viewing the DV, we removed any vasculature from the 3D image that terminated in a liver lobe. Using this technique, we were able to visualize only the UV, PV, and IVC (Fig. 3). The PV was identifiable as a smaller vessel running parallel with the IVC and meeting the UV in a region in which the major branches of each lobe converged. We also obtained an unobstructed view of the DV (Fig. 3B), which meets with the IVC, in transverse planes that are anterior to the PV/UV junction. In combination, these techniques illustrated proof of concept that serial reconstruction of histological sections could be used to identify the DV in neonatal mice.

Failure of DV Closure in *Ahr*-Null Mice. To determine whether the portocaval shunt in *Ahr*-null mice is a patent DV, we compared the ontogeny of this structure in wild-type and *Ahr*-null mice. To accomplish this, we generated 3D reconstructions from both mouse strains at neonatal ages, ranging from newborn to 48 h old. Because birth of a litter typically occurs over several hours, we performed caesarian derivations of pregnant female mice at embryonic day 18.5 to normalize the birth hour of newborn pups. Livers were collected, sectioned, stained, photographed, rendered, and reconstructed from mice sacrificed at 1, 6, 12, 18, 24, and 48 h after birth (as described above). The vascular structures of the reconstructions were then modified to emphasize only the PV, UV, IVC, and DV (as described above). These 3D images clearly show the presence of the DV at birth and 6 h of age in both wild-type (Fig. 4, A and B) and *Ahr*-null (Fig. 4, G and H) livers. In wild-type mice, the DV seems to have a more restricted diameter at 24 h of age (Fig. 4E) and the vessel disappears completely by 48 h of age (Fig. 4F). By contrast, the DV remains fully open through 48 h of age in the null mice (Fig. 4, G–L).

The 3D reconstructions illustrate a variety of shapes for the IVC, PV, and UV in these livers. These patterns reflect differences in the arrangement of the liver, kidneys, spleen, and intestines during fixation. Some variability in vessel morphology in the 3D images reflects subtle changes in liver shape caused by fixation. Despite efforts to control the spatial organization of the liver, some liver lobes spread out in fixative but others did not.

Cellular Composition of the DV Is Similar in *Ahr*-Null and Wild-Type Mice. Once evidence of a patent DV in *Ahr*-null mice was generated, the individual hematoxylin & eosin- stained slides containing this structure were examined for histological evidence of pathology at this site. This analysis was performed in several mice at ages ranging from 6 to 48 h of age. Measurements were typically taken from at least three individual mice at each time point. Although we were able to identify basophilic hematopoietic cells lining the DV of both normal and *Ahr*-null mice, we were unable to find clear differences in the cellular composition of the DV between these two strains between 6 and 24 h of age (Fig. 5).

Diameters of Major Intrahepatic Vessels Do Not Contract after Birth in *Ahr*-Null Mice. The 3D reconstructions were valuable for identification of the DV and for

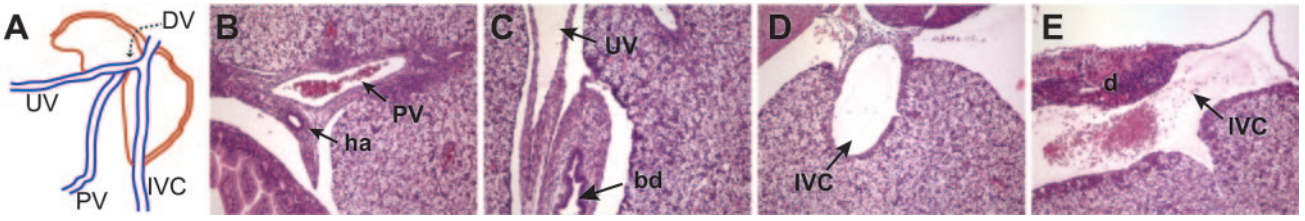

Fig. 1. The IVC, PV, and UV can be identified at entry to the liver. A, a schematic representation of major hepatic vessels including the PV, UV, and IVC. The fetal liver (thin red line) and diaphragm (thick red line) are also represented. B, the PV drains the gut and enters the liver between all of the lobes in association with the hepatic artery (ha). C, the UV enters the liver through the median lobe adjacent to the bile duct (bd). D, the infrahepatic IVC drains the renal veins and then enters the distal portion of the right posterior lobe. E, the IVC then traverses the right posterior lobe and exits through the diaphragm (d).

illustration that the DV closes in wild-type, but not *Ahr*-null mice. To compare vessel diameters in *Ahr*-null mice and wild-type control mice, we measured diameters in histological sections of age-matched livers at 6, 12, 24, and 48 h of age. Analysis of these data indicate that the wild-type UV diameter decreased from 212 to 106 μm ($p = 0.003$) from 6 to 48 h (Fig. 6, lower left). The PV diameter also decreased from 198 to 65 μm ($p = 0.0001$) in wild-type mice during this period (Fig. 6, upper left). Although not significant ($p = 0.12$), there was trend toward decreased diameter of the IVC in wild-type mice (170 to 101 μm) (Fig. 6, upper right).

In wild-type mice, the average lumen diameter of the DV decreased in size from 162 to 6 μm between the ages of 6 and 48 h (Fig. 6, lower right). Decreased DV diameter in wild-type mice was significant by as early as 12 h of age (162 to 62 μm, $p = 0.007$). At 24 h of age, we found resolution of only one DV among four wild-type mice. By 48 h of age, DV resolution was complete in 80% of the wild-type mice (four of five) examined. By contrast, the DV was fully patent in all *Ahr*-null mice at

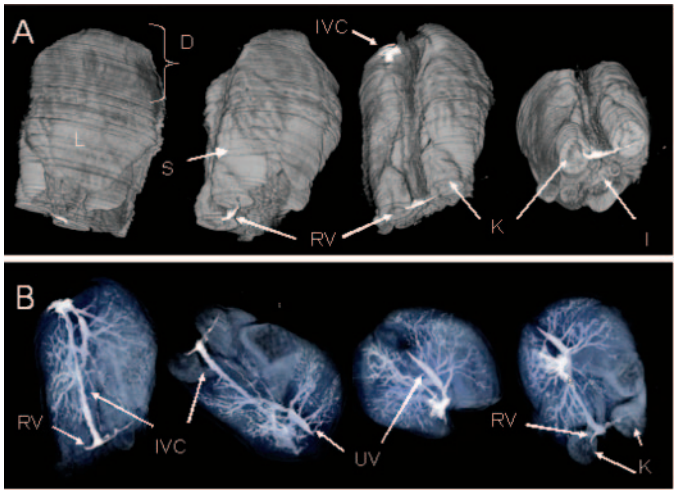

Fig. 2. 3D reconstructions identify the major vessels in a neonatal mouse liver in the context of liver morphology. Vascular patterns of the liver were reconstructed in three dimensions to highlight either organ morphology (A) or hepatic blood vessels (B) from several viewing perspectives. In A, we can see the liver lobes (L), which are obscured proximally by the diaphragm (D). We also see the spleen (S) and kidneys (K) inferior and posterior to the distal portions of the liver lobes. Intestines (I) are also visible. When organ surfaces are presented as "ghosts", the IVC, renal veins (RV), and UV become visible. In these reconstructions, the ductus venosus remains obscured by surrounding vessels. Supplemental Figs. 1 and 2 show Voxx-rendered videos of organ morphology from a mouse abdominal cavity and its hepatic vasculature, respectively.

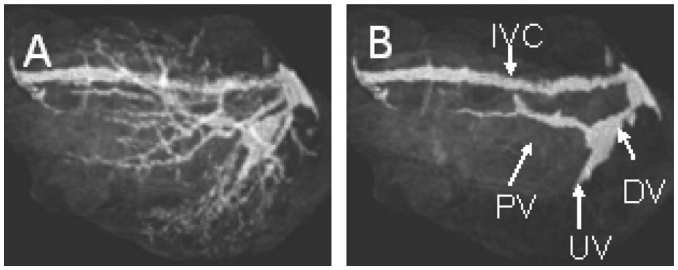

Fig. 3. Vascular reconstructions can be pruned to identify the DV. A, when all vessels greater than ~25 μm in diameter are highlighted, the DV remains obscured by surrounding vessels. B, to isolate the DV, we highlighted only the IVC, PV, and UV and the one vessel that connects them (DV). A and B show vascular patterns in 3D reconstructions that are projected in the same orientation.

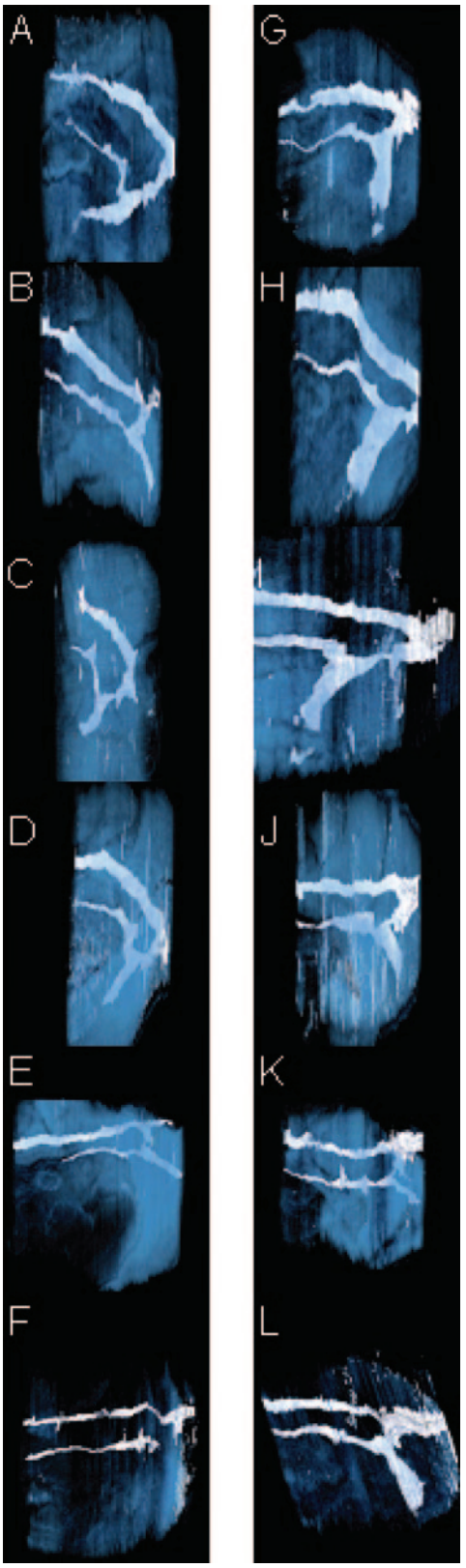

Fig. 4. Three dimensional reconstructions of the vascular network of wild-type and *Ahr*-null mouse livers. 3D reconstructions of major vessels of both wild-type (A–F) and *Ahr*-null (G–L) livers show resolution of the DV in wild-type but not *Ahr*-null mice over the first 48 h of age. Reconstructions were generated for mice of 1 (A and G), 6 (B and H), 12 (C and I), 18 (D and J), 24 (E and K), and 48 (F and L) hours of age. In wild-type mice, the DV is completely resolved by 48 h of age (F), whereas the DV remains fully patent in *Ahr*-null animals (L).

24 h (zero of four resolved) and at 48 h of age (zero of four resolved). Vessels in livers from null mice over the first 48 h did not change in diameter, resulting in significantly greater diameters of null versus wild-type vessels. At 48 h of age, vessel diameters of the *Ahr*-null PV ($p = 0.0064$), UV ($P = 0.0022$), and DV ($p = 0.0009$) were significantly greater than those of the wild-type control mice. IVC diameter was not significantly greater in *Ahr*-null livers at 48 h ($p = 0.1011$).

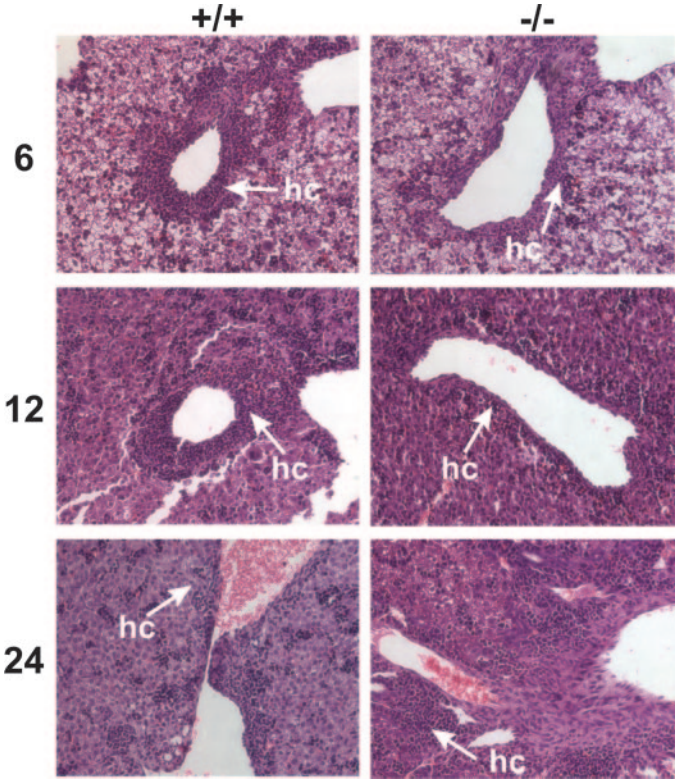

Fig. 5. Cellular composition of the DV is similar for wild-type and *Ahr*-null mice. Serial sections through the DV in wild-type (left) and *Ahr*-null (right) livers were evaluated to determine whether the histology of the DV was different in wild-type versus *Ahr*-null mice. Evaluation of DV histology at 6, 12, and 24 h of age show occasional areas of hematopoietic cells (hc), which seem more basophilic than the adjacent hepatocytes, in both wild-type and *Ahr*-null mice, but we found no consistent differences between alleles.

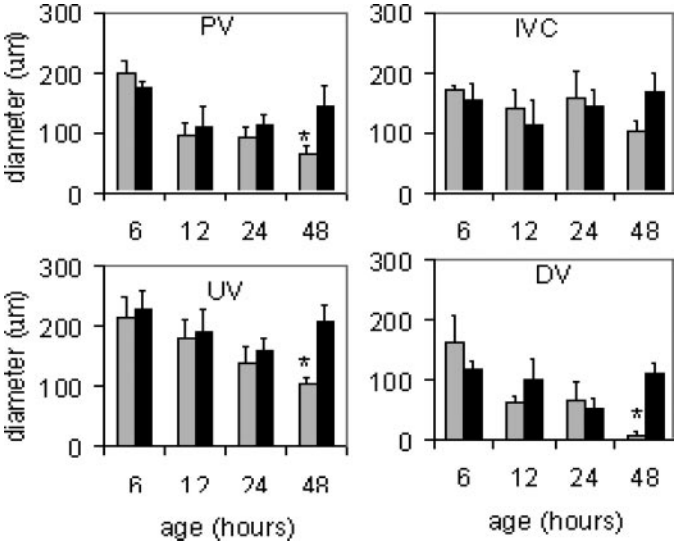

Fig. 6. Major veins of *Ahr*-null livers have increased diameters at 48 h of age. Diameters of the IVC, PV, UV, and DV were measured at specific points within the liver for an average of 3.8 mice per group at 6,12, 24, and 48 h of age. Vessel diameters for the PV, UV, IVC, and DV are plotted for wild-type (gray) and *Ahr*-null (black) mice. *, statistically significant at $P < 0.01$.

***Ahr*-Null and Wild-Type Mice Have Similar Vessel Diameters in the Brain.** Given that hepatic vessel diameter was increased in the *Ahr*-null animals, we wondered whether this phenotype was a generalized vascular phenomenon. Therefore, we set out to examine nonhepatic vessel diameters in the *Ahr*-null mouse at 48 h of age. To this end, we evaluated the morphology of capillaries and small vessels in identical regions of the mouse brain at 48 h of age. Blood vessels of *Ahr* heterozygous (Fig. 7A) and homozygous (Fig. 7B) null mice of 48 h of age were visualized by fluorescence microscopy. Capillary diameters were found to be equivalent in *Ahr*-null animals and their heterozygous control mice, with average diameters of 5.7 (S.D. = 0.26) and 5.5 μm (S.D. = 0.51), respectively. Likewise, small vessels in the *Ahr*-null mouse (90 μm, S.D. = 14.4) were similar in diameter to vessels in the wild-type control mouse (83 μm, S.D. = 4.6).

Discussion

Background. The purpose of this study was to examine the two most likely underlying causes of portocaval shunting in *Ahr*-null mice. We attempted to determine whether the shunt observed in adult *Ahr*-null mice represents the persistence of the fetal structure known as the DV or if it is the result of a distinct collateral blood vessel that arose from an independent process. To make this distinction, we generated 3D images of the developing vascular architecture from serial histological sections of the neonatal mouse liver and abdomen. Using this approach, we were able to reliably identify the PV, IVC, UV, and DV. We found that the DV normally closes within 48 h after parturition in wild-type mice but remains patent in *Ahr*-null animals. In previous reports, we postulated that this portocaval shunt might be a patent DV, but this is the first formal evidence that such a shunt exists and defines a congenital aberration inherent to the *Ahr*-null genotype. Our conclusion does not support conjecture that

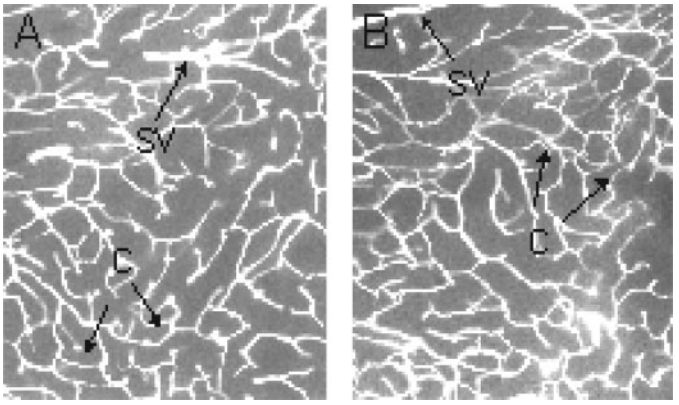

Fig. 7. Diameters of capillaries in brain are similar in *Ahr* heterozygous and homozygous null mice. Capillaries of *Ahr* heterozygous (A) and homozygous (B) null mice at 48 h of age were visualized by fluorescence microscopy. Capillaries (c) were identified by their consistently small diameter and were found to be equivalent in null and control animals. To measure small vessel diameters (sv), we identified a group of vessels in a small region of the brain near the substantia nigra and measured diameters for all of the vessels in this group.

the shunt represents an acquired structure generated later in life. Taken in sum, these data provide compelling evidence that the AHR plays an important role in the normal development of the hepatic vascular architecture, with a hallmark effect of the null phenotype being failure of DV closure.

Advantages of 3D Imaging by Serial Reconstruction. Three-dimensional reconstruction of the developing vascular architecture required extensive tissue sectioning and use of novel computer software. Yet the 3D images provide considerable power and flexibility and hold the potential to yield a vast amount of information about vascular morphology and the relationship between blood vessel position and organ morphology. The power of this approach is that it allows the image to be turned along any axis (*X*, *Y*, or *Z*) for more careful examination of the relationships between different blood vessels and surrounding structures (Fig. 2). We can thereby identify and follow the PV, IVC, and UV into the neonatal liver lobes. Such tracking was essential to formally and reproducibly define the DV. Upon examining livers from mice 6 to 48 h after birth, we rapidly and conclusively identified the DV from adjacent branches of the major vessels and were able to characterize its anatomy and how it changed over time relative to other vascular and histological features.

Although considerable technical hurdles had to be overcome, we chose to employ the 3D reconstruction approach over more classic approaches of vascular imaging. In the past, vascular architecture has often been visualized in 3D by perfusion of plastic resins into tissues, followed by digestion of surrounding parenchyma to create a cast or physical model of the intravascular space (Mironov et al., 1994; Kondo, 1998; Lahvis et al., 2000; Navarro et al., 2003). The advantages of 3D reconstruction from serial sections over latex cast methods are multiple. First, unlike latex casts, the 3D images generated by reconstruction are digitized and thus are readily viewed, archived, and shared among investigators. Second, unlike latex casts, the reconstruction approach is derived from histological sections, so we have the unique ability to model the architecture of a vascular structure, identify a region of interest, and re-examine the corresponding sections at high magnification. This capacity allows study of the cellular or molecular characteristics of the vascular feature of interest (e.g., Fig. 5). In latex casts, such material is removed. Finally, latex casts of complex vascular structures are often difficult to interpret in regions in which vascular structures are dense or intersect. In the 3D reconstruction approach, such regions can be examined after digital pruning of overlapping or intersecting structures that obscure a region of interest (e.g., Fig. 3).

We find that 3D reconstructions generated from histological sections provide advantages that cannot be obtained from noninvasive imaging modalities, such as microscopic computed tomography, positron-emission tomography, or magnetic resonance imaging. Noninvasive modalities do not yet provide information regarding cell composition and gene expression at levels of resolution that are readily achieved with light microscopy (Huang et al., 1996; Kantor et al., 2000; Sharma et al., 2002). It is noteworthy that 3D reconstructions also provide advantages for vascular imaging that cannot be obtained from confocal and multiphoton microscopy, which generate 3D images limited to a few hundred microns in section thickness (Phillips et al., 2001). To reconstruct vascular patterns that exist throughout an organ, even confocal and multiphoton microscopy would require 3D reconstruction from multiple sections, as performed here.

Mechanism of DV Closure and Patency. The mechanism of DV closure is likely to be distinct from that for closure of the ductus arteriosus (DA). Resolution of the DA involves a rapid "functional constriction" followed by "anatomic closure", which permanently removes the vessel (Smith, 1998). The DV is unlikely to undergo functional constriction because an elastin-mediated sphincter has not been identified within the DV of humans or dogs (Burton and White, 1999; Mavrides et al., 2002). Such a structure was also not observed here. The difference in the timing of closure is also different. In humans, functional constriction results in DA closure within 3 days of birth (Alenick et al., 1992), whereas in humans the DV requires more than 2 weeks to resolve (Fugelseth et al., 1999). Additional evidence that these structures close by different mechanisms is that the DA is resolved in adult *Ahr*-null mice (Lahvis et al., 2000) but that the DV remains patent in this same mutant strain.

We were interested in the possibility that the mechanism for resolution of the DV resembles that of neonatal capillary beds. In mammals, many small neonatal vessels close within 3 weeks after birth, including arteriovenous shunts on the brain surface (Wang et al., 1992; Feher et al., 1996; Krolo and Hudetz, 1998), membrane capillaries and vitreal arteries of the eye (Lang and Bishop, 1993; Mitchell et al., 1998; Ito and Yoshioka, 1999), lung capillaries (Zeltner and Burri, 1987), and liver sinusoids (Mccuskey et al., 1997; Kiserud, 2001). In the neonatal eye, resolution of capillaries of the papillary membrane is thought to be caused by macrophage accumulation (Lang and Bishop, 1993; Ito and Yoshioka, 1999), resulting in reduced blood flow, localized ischemia, vascular endothelial growth factor (VEGF0 deprivation (Meeson et al., 1999), and endothelial cell apoptosis (Meeson et al., 1996; Meeson et al., 1999). Our data are inconsistent with macrophage accumulation as an essential step in DV closure, in that histological analysis did reveal evidence of large numbers of macrophages adjacent to the DV in normal development.

We have previously noted vascular changes in other organs of the *Ahr*-null mouse, including a persistent hyaloid artery, expansion of limbal vessels of the eye, and altered vascular density of the kidney. Whether these vascular alterations are a direct result of the lack of AHR signaling or are a consequence of altered vascular flow caused by the patent DV cannot be determined from these studies. However, it is clear that the vascular changes resulting from an *Ahr*-null allele occur in a number of organ systems yet do not seem to extend to every organ system.

The results that have arisen from this 3D image analysis through development have led us to speculate on a mechanism to explain the patent DV in *Ahr*-null mice. In this regard, we observed that wild-type neonatal hepatic vessels constrict by approximately the second day after birth. Yet, this developmentally mediated constriction does not occur as robustly in *Ahr*-null mice. Our data suggest that hepatic vessel constriction is attributable to some aspect of AHR signaling. In mice harboring the *Ahr*-null allele, this receptor-mediated event is lost, leading to increased vasodilation and inefficient DV closure.

Summary. Using 3D reconstructions from serial histological sections, we have been able to evaluate hepatic vascular

development in the neonatal mouse. Our approach allowed us to evaluate DV closure within the context of whole organ vascular patterns, as well as view this biology within the context of neighboring cellular constituents. Our results demonstrate that the *Ahr* is necessary for resolution of the DV, a shunt that normally closes within 2 days after birth in mice. This aberration in early vascular development in *Ahr*-null mice rules out the alternative explanation that an acquired shunt emerged later in life. These data also lend support to the hypothesis that normal DV closure is related to a generalized postpartum decrease in the diameter of the major vessels of the liver. The inefficiency of this neonatal vasoconstriction may explain the failure of DV closure in *Ahr*-null mice.

Acknowledgments

Three-dimensional images in Figs. 2, 3, and 5 were generated by with Voxx by Jeffrey L. Clendenon at the Indiana Center for Biological Microscopy, Indiana University School of Medicine. We thank Jacqueline Walisser for assistance in manuscript preparation.

References

Alenick DS, Holzman IR, and Ritter SB (1992) The neonatal transitional circulation: a combined noninvasive assessment. *Echocardiography* **9:**29–37.
Burton CA and White RN (1999) The angiographic anatomy of the portal venous system in the neonatal dog. *Res Vet Sci* **66:**211–217.
Clendenon JL, Phillips CL, Sandoval RM, Fang S, and Dunn KW (2002) Voxx: a PC-based, near real-time volume rendering system for biological microscopy. *Am J Physiol* **282:**C213–C218.
Datta DV, Grover SL, Saini VK, Datta BN, Aikat BK, and Chhuttani PN (1975) Portal hypertension in chronic leukaemia. *Br J Haematol* **31:**279–285.
Feher G, Schulte ML, Weigle CG, Kampine JP, and Hudetz AG (1996) Postnatal remodeling of the leptomeningeal vascular network as assessed by intravital fluorescence video-microscopy in the rat. *Brain Res Dev Brain Res* **91:**209–217.
Fugelseth D, Kiserud T, Liestol K, Langslet A, and Lindemann R (1999) Ductus venosus blood velocity in persistent pulmonary hypertension of the newborn. *Arch Dis Child Fetal Neonatal Ed* **81:**35–39.
Huang W, Plyka I, Li H, Eisenstein EM, Volkow ND, and Springer CS Jr (1996) Magnetic resonance imaging (MRI) detection of the murine brain response to light: temporal differentiation and negative functional MRI changes. *Proc Natl Acad Sci USA* **93:**6037–6042.
Ito M and Yoshioka M (1999) Regression of the hyaloid vessels and pupillary membrane of the mouse. *Anat Embryol* **200:**403–411.
Kantor B, Ritman E, Holmes D, and Schwartz R (2000) Imaging angiogenesis with three-dimensional microscopic computed tomography. *Curr Intervent Cardiol Rep* **2:**204–212.
Kiserud T (2001) The ductus venosus. *Semin Perinatol* **25:**11–20.
Kondo S (1998) Microinjection methods for visualization of the vascular architecture of the mouse embryo for light and scanning electron microscopy. *J Electron Microsc* **47:**101–113.
Krolo I and Hudetz AG (1998) Remodeling of the leptomeningeal microvascular plexus in neonatal rats. *Adv Exp Med Biol* **454:**349–354.
Lacroute P and Levoy M (1994) Fast volume rendering using a shear-warp factorization of the viewing transformation, in *SIGGRAPH 94: Proceedings of the 21st Annual Conference on Computer Graphics and Interactive Techniques*; 1994 Jul 24–29; Orlando, FL. p. 451–458, ACM Press, New York, NY.
Lahvis GP, Lindell SL, Thomas RS, McCuskey RS, Murphy C, Glover E, Bentz M, Southard J, and Bradfield CA (2000) Portosystemic shunting and persistent fetal vascular structures in aryl hydrocarbon receptor-deficient mice. *Proc Natl Acad Sci USA* **97:**10442–10447.
Lang RA and Bishop JM (1993) Macrophages are required for cell death and tissue remodeling in the developing mouse eye. *Cell* **74:**453–462.
Mavrides E, Moscoso G, Carvalho JS, Campbell S, and Thilaganathan B (2002) The human ductus venosus between 13 and 17 weeks of gestation: histological and morphometric studies. *Ultrasound Obstet Gynecol* **19:**39–46.
McCuskey RS, Ekataksin W, LeBouton AV, Nishida J, Krasovich MA, McDonnell D, Williams C, and Koldovsky O (1997) Development of hepatic sinusoidal structure and function in suckling rats, in *Cells of the Hepatic Sinusoid VI* (Wisse E, Knook DL, and Balabaud C, eds), pp. 67–70, Kupffer Cell Foundation, Leiden, the Netherlands.
McDonald DM, Thurston G, and Baluk P (1999) Endothelial gaps as sites for plasma leakage in inflammation. *Microcirculation* **6:**7–22.
Meeson A, Palmer M, Calfon M, and Lang R (1996) A relationship between apoptosis and flow during programmed capillary regression is revealed by vital analysis. *Development* **122:**3929–3938.
Meeson AP, Argilla M, Ko K, Witte L, and Lang RA (1999) VEGF deprivation-induced apoptosis is a component of programmed capillary regression. *Development Suppl* **126:**1407–1415.
Mimura J and Fujii-Kuriyama Y (2003) Functional role of AhR in the expression of toxic effects by TCDD. *Biochim Biophys Acta* **1619:**263–268.
Mironov V, Hritz MA, LaManna JC, Hudetz AG, and Harik SI (1994) Architectural alterations in rat cerebral microvessels after hypobaric hypoxia. *Brain Res* **660:**73–80.
Mitchell CA, Risau W, and Drexler HC (1998) Regression of vessels in the tunica vasculosa lentis is initiated by coordinated endothelial apoptosis: a role for vascular endothelial growth factor as a survival factor for endothelium. *Dev Dyn* **213:**322–333.
Navarro M, DeRuiter MC, Carretero A, and Ruberte J (2003) Microvascular assembly and cell invasion in chick mesonephros grafted onto chorioallantoic membrane. *J Anat* **202:**213–225.
Phillips CL, Arend LJ, Filson AJ, Kojetin DJ, Clendenon JL, Fang S, and Dunn KW (2001) Three-dimensional imaging of embryonic mouse kidney by two-photon microscopy. *Am J Pathol* **158:**49–55.
Sharma V, Luker GD, and Piwnica-Worms D (2002) Molecular imaging of gene expression and protein function in vivo with PET and SPECT. *J Magn Res Imaging* **16:**336–351.
Smith GC (1998) The pharmacology of the ductus arteriosus. *Pharmacol Rev* **50:**35–58.
Sokal RR and Rohlf FJ (1995) Biometry: the principles and practice of statistics in biological research, 3rd ed, W. H. Freeman and Co., New York.
Sugiura N, Karasawa E, Saotome N, Miki M, Matsutani S, and Ohto M (1992) Portosystemic collateral shunts originating from the left portal veins in portal hypertension: demonstration by color Doppler flow imaging. *J Clin Ultrasound* **20:**427–432.
Wang DB, Blocher NC, Spence ME, Rovainen CM, and Woolsey TA (1992) Development and remodeling of cerebral blood vessels and their flow in postnatal mice observed with in vivo videomicroscopy. *J Cereb Blood Flow Metab* **12:**935–946.
Zeltner TB and Burri PH (1987) The postnatal development and growth of the human lung. II. Morphology. *Respir Physiol* **67:**269–282.

Address correspondence to: Christopher A. Bradfield, McArdle Laboratory for Cancer Research, 1400 University Ave., Madison, WI 53706. E-mail: bradfield@oncology.wisc.edu